

ARMY RESEARCH LABORATORY



# An Experimental Examination of the Streamwise Velocity in a Plane Mixing Layer using a Single Hot-Wire Sensor

by Richard B. Loucks

ARL-TR-1391

September 1997

DTIC QUALITY INSPECTED 2

19971223 093

Approved for public release; distribution unlimited.

The findings in this report are not to be construed as an official Department of the Army position unless so designated by other authorized documents.

Citation of manufacturer's or trade names does not constitute an official endorsement or approval of the use thereof.

Destroy this report when it is no longer needed. Do not return it to the originator.

# Army Research Laboratory

Adelphi, MD 20783-1197

---

ARL-TR-1391

September 1997

---

## An Experimental Examination of the Streamwise Velocity in a Plane Mixing Layer using a Single Hot-Wire Sensor

Richard B. Loucks

Information Science and Technology Directorate

---

## Abstract

---

A single-sensor hot-wire probe was used to make streamwise measurements in a turbulent plane mixing layer. The mixing layer, with a velocity ratio of approximately 2:1, was created in an open return wind tunnel by the insertion of a curved splitter plate. Conditions were studied with the splitter plate boundary layers tripped. The single-sensor results demonstrate that this mixing layer has standard velocity field statistical properties. The data were taken at several Reynolds numbers in the fully turbulent flow downstream of the mixing point. The results from the tripped initial boundary layers/fully turbulent conditions were compared with the temporally developing mixing layer direct numerical simulation results of Rogers and Moser (1994).

## Contents

<b>1. Introduction .....</b>	<b>1</b>
<b>2. Background .....</b>	<b>1</b>
2.1 <i>Experimental Characteristics</i> .....	2
2.2 <i>Numerical Simulations</i> .....	4
<b>3. Experiment Program .....</b>	<b>5</b>
3.1 <i>Preliminary Characterization</i> .....	6
3.1.1 <i>Initial Computational Analysis</i> .....	6
3.1.2 <i>Final Design of Insert</i> .....	8
3.1.3 <i>Flow Visualization</i> .....	9
3.2 <i>Hot-Wire Measurements</i> .....	9
3.2.1 <i>Measurement Results</i> .....	10
3.2.2 <i>Initial Conditions</i> .....	17
3.3 <i>Roller Passage</i> .....	20
<b>4. Conclusions and Recommendations .....</b>	<b>22</b>
<b>5. References .....</b>	<b>22</b>
<b>Distribution .....</b>	<b>27</b>
<b>Report Documentation Page .....</b>	<b>31</b>

## Figures

1. Mixing layer velocity profile .....	2
2. Two-dimensional calculations of flow around insert in tunnel .....	7
3. UMCP wind tunnel insert .....	8
4. Streaklines from smoke shown using flashbulb with 200-ASA film .....	10
5. Contour results of single hot-wire measurements .....	11
6. Growth of vorticity thickness .....	14
7. Growth of momentum thickness .....	15
8. Normalized mean velocity profiles .....	16
9. Normalized Reynolds normal stress in streamwise direction .....	16
10. Initial streamwise profiles .....	17
11. Boundary layer profile of expansion surface .....	18
12. Boundary layer profile of tripped contraction .....	20
13. Sample data and normalized spectrum .....	21

## Tables

1. Characterization results .....	13
2. Turbulent boundary layer .....	20

# 1. Introduction

The purpose of this research was to obtain a thorough knowledge of the structure and dynamics of the streamwise velocity of a plane mixing layer using a single-sensor hot-wire probe, developed in the Turbulence Research Laboratory (TRL) at the University of Maryland College Park (UMCP). The results of the measurements were compared against a theoretical computation of a similar flow by Rogers and Moser (1994).

The turbulent plane mixing layer is technically one of the most important types of generic turbulent flows. It is the basic flow field created to enhance species mixing for combustion devices. The turbulent mixing layer is also the underlying flow in many types of fluid instability problems. The results of this project could lead to an improvement in state-of-the-art turbulence models used in computational fluid dynamics for calculating drag and mixing.

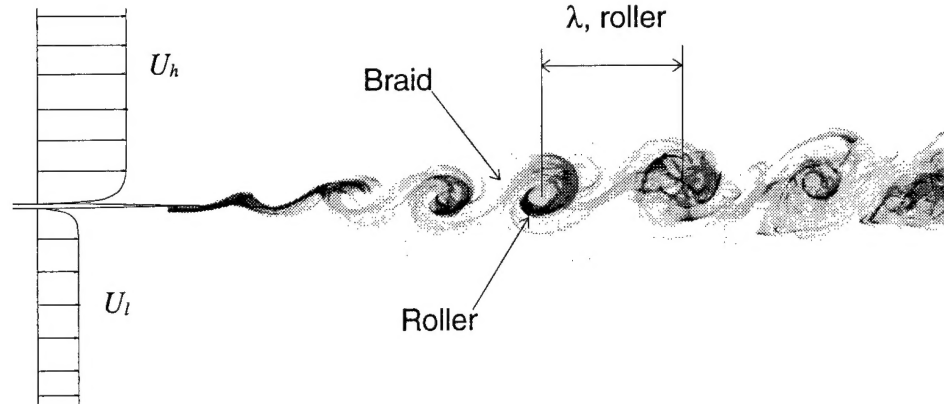
# 2. Background

Plane mixing layers have been widely studied, both experimentally (Bradshaw, 1966; Wygnanski and Fiedler, 1970; Miksad, 1972; Batt, 1977) and computationally (Patnaik, Sherman, and Corcos, 1976; Riley and Metcalf, 1980; Jacobs and Pullin, 1989). After the realization by Brown and Roshko (1974) that coherent structures dominate some of the mixing dynamics, a large effort was undertaken to investigate these structures in an effort to further understand the onset and evolution of turbulence.

Mixing layers play an important part in many engineering applications: they govern the rate of mixing in flow reactors and combustion chambers, and they are the dominant cause of noise from modern aircraft propulsion systems. Mixing layers are also of interest because they exhibit self-similar behavior. At sufficiently high Reynolds numbers, the mixing layer tends to grow linearly, and the shapes of the mean velocity and turbulence profiles are independent of downstream distance when scaled with appropriate local length and velocity scales.

The region between the parallel streams is most likely the simplest free shear flow that can be studied since the driving flows,  $U_h$  and  $U_l$ , are constant throughout. It is easily reproduced in a wind tunnel and creates large coherent turbulent structures in a boundary-free field. A large body of experimental and numerical results has demonstrated that the mixing layer developed by the meeting of two streams at the end of a splitter plate, as depicted in figure 1, is dominated by mostly two-dimensional spanwise vortex structures rising from the Kelvin-Helmholtz instability of the layer (Brown and Roshko, 1974; Winant and Browand, 1974; Corcos and Sherman, 1984; Metcalf, Hussain, Menon, and Hayakawa, 1987; Huang and Ho, 1990). These structures, referred to as "rollers," are evenly spaced by some length  $l$ , and convect downstream at a constant velocity, but grow in size. Eventually, some rollers interact by rotating about each other.

Figure 1. Mixing layer velocity profile.



These interacting rollers will pair, forming a single vortex with double the original spacing. Pairing occurs repeatedly, controlling the growth rate of the mixing layer.

## 2.1 Experimental Characteristics

Brown and Roshko (1974), who first recognized the rollers, recorded their observations with a series of shadowgraphs. They showed that the roller persisted down the length of their test region. Since the mean velocity profiles seemed self-preserving and the spread rate was linear, Brown and Roshko suggested that this was the unique, fully developed form of a turbulent mixing layer. They also observed that some rollers would merge, or pair, and evolve into a single roller. Winant and Browand (1974) discovered that at low Reynolds numbers, self-preservation was maintained even after several stages of vortex pairings, without complete breakdown to fully turbulent flow. Dimotakis and Brown (1976) found evidence of the roller structures at high Reynolds numbers. Chandrsuda, Mehta, Weir, and Bradshaw (1978) speculated that the rollers in the mixing layer existed only if the free-stream turbulence was low. They rationalized that high turbulence in the free stream caused the rollers to break down early, and significantly high free-stream turbulence would not allow the rollers to form at all. They also suggested that the rollers were not a universal feature of the mixing layer, and that pairing could happen along part, but not all, of the span of the roller. Browand and Troutt (1980) learned that the rollers quickly approached an asymptotic state, where the lateral correlation length became proportional to the local mixing length (momentum thickness). They also observed spanwise irregularities, but argued that these irregularities were a product of pairing.

Briedenthal (1981) visualized the development of the rollers with an aqueous, diffusion-limited reaction. He observed that a transition occurred in which the product of the reactants increased by an order of magnitude. He attributed this transition to the development of small-scale, three-dimensional motions in the flow. Downstream of the transition, the degree of mixing became independent of the local Reynolds number. Hernan and Jimenez (1982) observed that most of the entrainment of the free-stream fluid occurred during the normal life of the rollers, and not during pairing.

Ho and Huang (1982) discovered they could change the growth rate of the rollers with subharmonic perturbation by forcing several of the rollers to merge simultaneously. This agreed with Kelly (1967), who proposed that a subharmonic resonance mechanism could feed energy to large wavenumber structures, and with Pierrehumbert and Widnall (1982), who determined that an array of rollers were unstable to subharmonic disturbances. Jiminez (1983) concentrated on studying some streamwise irregularities that appeared on the rollers, and concluded that these irregularities were a secondary instability and actually deformed the large roller. Lang (1985) measured the instantaneous values of the streamwise and transverse velocity components, spanwise vorticity, and the Reynolds stress. He discovered that the spanwise vorticity component had values opposite to the sense of the mean vorticity most of the time.

Bernal and Roshko (1986) expanded the study of the secondary structures with both gas and water facilities. They observed the same type of streaks seen earlier by Brown and Roshko (1974). By visualizing a plane normal to the streamwise direction with the use of laser-induced fluorescence, Bernal and Roshko visualized the secondary instabilities and concluded that these instabilities were streamwise vortices superimposed on the rollers. A chemically reacting mixing layer was used by Lasheras, Cho, and Maxworthy (1986) to visualize and investigate the streamwise vortices. They determined that these streamwise vortices were a product of upstream perturbations, and could be increased in intensity by further perturbing the upstream flow. The streamwise vortices seemed to originate in the braid region between the rollers. The study concluded that the streamwise vortices seemed to have a scale, as measured by the size of the cores, smaller than but comparable to that of the roller's cores; this they significantly contributed to the entrainment process in the early stages of the mixing layer development. Lasheras and Choi (1988) performed a similar experiment, except they introduced a sinusoidal perturbation by corrugating the splitter plate and indenting the splitter plate edge. They showed that the mixing layer with induced streamwise vorticity grew at a greater rate than the flow without induced streamwise vorticity. It was again surmised that the streamwise vortices originated within the braid region. The study concluded that the perturbed vorticity existing within the braids underwent axial stretching from the effect of the strain field created by the evolving rollers. This resulted in the formation of vortex tubes whose axes were aligned with the principle direction of the positive strain field.

Balint, Wallace, and Vukoslavcevic (1989) demonstrated the ability to measure velocity and vorticity directly with the use of a nine hot-wire anemometer array. They were able to collect data at a single station within the shear layer, at the edge of the layer, and in the free stream. The dominant source term in the enstrophy balance was due to vortex stretching from the fluctuating strain rate.

Bell and Mehta (1990) evaluated the development of the mixing layer originating from tripped and untripped boundary layers. The distance to achieve self-preservation was shorter for the tripped case, while the mix-

ing layer growth was greater for the untripped case. Bell and Mehta attributed this difference to the presence of streamwise vortices that added to the entrainment of the mixing layer. Bell, Plesniak, and Mehta (1992) performed a spanwise averaging of the mixing layer and found large variations in the mean flow and turbulence properties. They postulated that the variations were caused by the presence of spatially stationary streamwise vortices that ride along the rollers. They cautioned that there could be significant misinterpretations regarding the development of the mixing layer based on centerline data alone and proposed that subsequent discrepancies of past observances regarding growth rates and turbulence properties could be explained by the lack of spanwise averaging.

## 2.2 Numerical Simulations

Corcos and Sherman (1984) simulated the two-dimensional evolution of the roller using pseudo-spectral methods, and were able to simulate pairings. Corcos and Lin (1984) showed that the rollers were unstable due to three-dimensional disturbances that resulted in their deformation and the formation of the streamwise vortices in the braid region. Ashurst and Meiburg (1988) simulated the mixing layer using a discrete vortex method. They included two signs of vorticity to account for the weak boundary layer leaving the splitter plate. The result was a simulation in closer agreement with experimental observations. Ashurst and Meiburg were able to show the generation of streamwise vortices originating within the braid region. Ghoniem and Heidarinejad (1991) found that there was a strong similarity between the distribution of product concentrate and vorticity at a wide range of Damkohler numbers (the Damkohler number is the ratio between convective flow and chemical reaction times). They attributed the similarity to the entrainment associated with pairing.

Moser and Rogers (1991, 1992, 1993) performed several direct numerical simulations with a variety of initial conditions. They observed that pairing the rollers caused them to undergo a transition to small-scale turbulence. Pairing inhibited the growth of infinitesimally small disturbances and triggered the transition to turbulence in highly three-dimensional flow. They concluded that streamwise vortices were part of the initial cascade to small-scale turbulence. They also found that, in the self-preserving regime, the streamwise vortices were absent, and the mixing layer growth was reduced.

Rogers and Moser (1992) studied in great detail the origination and evolution of the streamwise vortices, also referred to as "rib" vortices. They found that the spanwise structures evolved into a corrugated roller, which was consistent with the observations of Jimenez (1983), with vortex stretching creating strong spanwise vorticity in a cup-shaped region at the bends of the rollers. For strong initial perturbations, the rib vortices collapsed into tight axisymmetric vortices. The rib vortex lines connected to other nearby rib vortices, and were kinked in the direction opposite to the roller vortex direction. Confirming earlier observations of Metcalf, Orszag, Brachet, Menon, and Riley (1987), and Huang and Ho (1990), Rogers and

Moser found that pairing prevented the growth of three-dimensionality by halting oversaturation.

Using a turbulent boundary layer simulation (Spalart, 1988) as the mixing layer initial condition, Rogers and Moser (1994) performed three simulations, one without any disturbance in the initial conditions, and the other two with varying disturbances in the initial conditions. They found that, after a development stage, the case with weak and no initial disturbance evolved in a self-preserving manner. This self-similar period was characterized by the absence of roller pairings, a lack of rib vortices in the braid region, and scalar mixing characterized by "marching" probability density functions (PDFs) (the largest probable value varies across the mixing layer, with the largest probable value on each side of the mixing layer being closer to the free-stream value of that side). The simulation using the strong initial disturbance approached self-preservation, but demonstrated strong organized pairings of the rollers, clearly defined regions within the braids of strong streamwise vorticity, and scalar PDFs that were "nonmarching." The statistics and structures from several experiments were in better agreement with the results of the simulations that did not exhibit organized pairings.

### 3. Experiment Program

Clearly, research on planar mixing layers has been quite extensive for over 20 years. Fortunately, state-of-the-art development in hot-wire anemometry has more recently allowed reasonably well-resolved instantaneous measurements of the velocity vector, vorticity vector, and strain rate tensor (Vukoslavcevic, Wallace, and Balint, 1991). This development provided the opportunity to obtain new information regarding aspects of turbulent phenomena within the mixing layer. To date, much of the experimentally measured data have concentrated on the streamwise and transverse velocities, the associated stresses, and the spanwise vorticity. Except for visual observations, there was little qualitative information and very few quantitative measurements of the secondary vortical structures, much less any statistical information related to their origin and evolution. There is a database of direct numerical simulations that provides considerable information (see work by Rogers and Moser). The conclusions drawn from these numerical simulations needed to be verified experimentally and, if possible, extended.

I modified the wind tunnel in the TRL at UMCP with a special insert, similar in design to the one used successfully by Dimotakis et al. (1976) and Lang (1985). The insert separated the conditioned flow coming from the wind tunnel contraction, accelerating the flow on one side while decelerating it on the other. The end of the insert provided a smooth meeting of the two laminar flows, with a velocity ratio of approximately 2:1, and created a mixing layer.

A series of single-sensor anemometer measurements and flow visualizations were made to determine if the turbulence characteristics of the mixing layer were consistent with the literature. Specifically, the goal was to match as closely as possible the simulated conditions of Rogers and Moser (1994). To evaluate the characteristics of the wind tunnel facility, a series of measurements were made with a single hot-wire anemometer traversing the mixing layer. The information obtained from the sensor was resolved to determine the turbulence statistical characteristics, including moments and one-dimensional spectra.

### 3.1 Preliminary Characterization

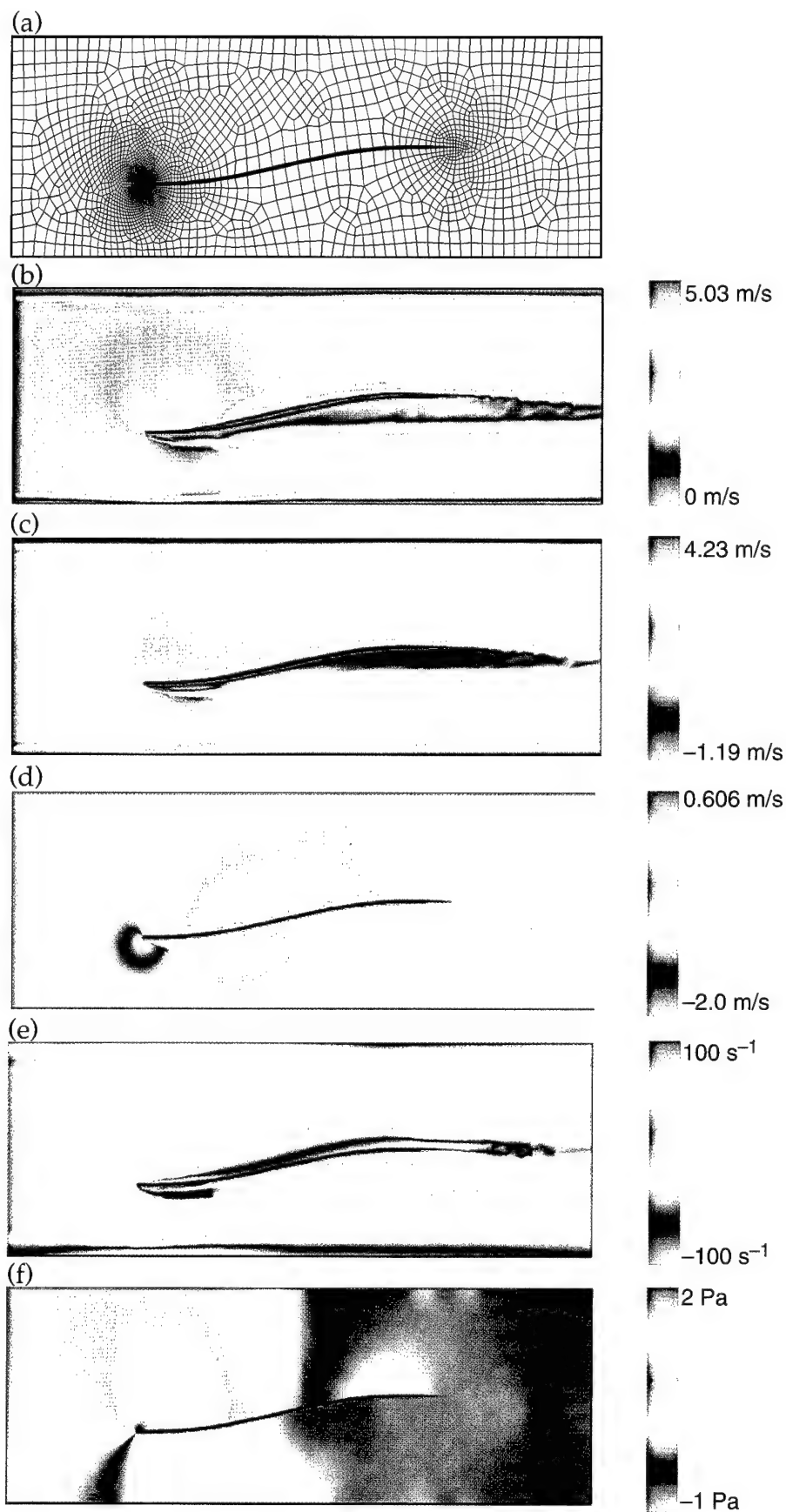
Following the method described by Dimotakis et al. (1976) and Lang (1985), and used in the GALCIT Facility, an insert for the wind tunnel at the UMCP's TRL was designed, fabricated, and installed. I obtained a series of single hot-wire measurements to evaluate the ability of the insert/wind-tunnel facility to generate a planar mixing layer.

#### 3.1.1 *Initial Computational Analysis*

To optimize the design of the insert, I performed a numerical computation of a two-dimensional, steady flow using a commercial software called ALGOR™ (1992). I believed this would give a reasonable approximation of the flow to be encountered. The model consisted of 3746 elements and was solved on a Pentium-processor PC in about 12 hours using the Penalty Parameter Method (ALGOR, 1992). I used a uniform flow of 1 m/s as the input boundary condition on the left side, and enforced the no-slip condition along the top and bottom surfaces of the insert. I used a rounded leading edge for the calculation, which helped fix the location of the leading edge stagnation point and reduced the chance of separation. The calculation was a pseudo-steady-state calculation; therefore the rollers would not appear in the results. Figure 2 shows the model's mesh, the results of the calculations of velocity magnitude, streamwise and transverse velocity components, vorticity, and pressure. The flow is represented moving from left to right. The color bar on the right of each plot shows the spatial variation of each flow component.

Figure 2f shows that an unequal pressure distribution exists along the entrance plane. The pressure drops a great deal as it passes below the insert. Above the insert, the pressure does not drop as much, similar to the pressure distribution at a contraction. This difference in pressure distribution drives the incoming fluid down into the lower pressure region. This produces a strong negative vertical component to the velocity vector, as seen in figure 2d. The vorticity in figure 2e also indicates that an area of recirculation exists at the lower insert entrance. The change in the streamwise velocity component in the transverse direction is very small, away from the insert and walls. A transverse change in the streamwise velocity compo-

Figure 2. Two-dimensional calculations of flow around insert in tunnel: (a) model mesh, (b) velocity magnitude, (c) streamwise velocity component, (d) transverse velocity component, (e) spanwise vorticity, and (f) pressure.



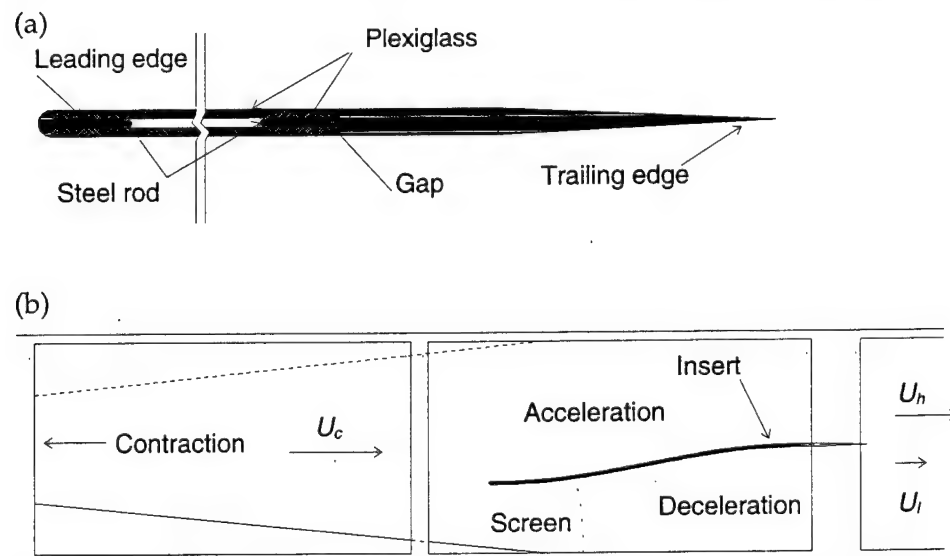
ment results in changes in the spanwise vorticity. The largest changes in vorticity occur at the leading edge of the insert and along the convex curved section. The resulting angle of attack of the flow around the leading edge forms a separation bubble at the low side of the leading edge. As a result, the insert acts as a bluff body, with a weak separation bubble filling the concave region of the expansion. The streamwise velocity is accelerated, as shown in figure 2c, as the fluid passes the insert. There is little difference in the free-stream velocities downstream of the splitter plate.

The simulation exposes a serious deficiency in the insert design. Fortunately, Dimotakis et al. (1976) and Lang (1985), who encountered the same problem, eliminated the separation at the leading edge by placing a flow restriction in the expansion side. In this manner, they were able to match inlet and outlet pressures. They placed perforated plates with 50-percent blockage on the expansion side, where separation might otherwise occur. The plates were curved to approximately follow the shape of a potential flow line of an inviscid flow through the expansion. Fine adjustments of the pressure drop were accomplished with an identical perforated plate placed over the first. Sliding one plate vertically relative to the other varied the percent blockage. This caused a small problem in that the flow direction was slightly changed, and this had to be accounted for by tilting the plate. Lang (1985) found that by reducing the blockage near the insert, the boundary layer could be made smaller at the end of the expansion.

### 3.1.2 Final Design of Insert

An insert was fabricated from two 0.00318-m (1/8-in.) thick sheets of plexiglass, each  $1.22 \times 0.91$  m. A semi-circular leading edge and tapering trailing edge were used to connect the sheets, as shown in figure 3a. Six 0.00318-m diam. steel rods passed through the gap in the plexiglass sheets and secured the insert to the wind tunnel walls. The insert was placed in the upstream part of the wind tunnel, about 2 m downstream of the end of the contraction. As shown in figure 3b, the insert served to separate the

Figure 3. UMCP wind tunnel insert: (a) components and (b) placement.



flow, accelerating the flow on one side and decelerating it on the other. The downstream part of the insert served as the splitter plate, and tapered to a sharp point with an angle of  $3.80^\circ$  on either side. The insert splits the flow such that there is a velocity ratio of about 2:1 at the splitter plate exit plane.

It was clear that a flow restriction on the deceleration side was necessary to equalize the pressure at the insert entrance plane. As shown in figure 3b, a screen of about 38 percent blockage was placed at the most likely point of separation on the deceleration side for two reasons: to equalize the pressure differential across the insert and to prevent flow separation in the region of adverse pressure gradient.

### 3.1.3 *Flow Visualization*

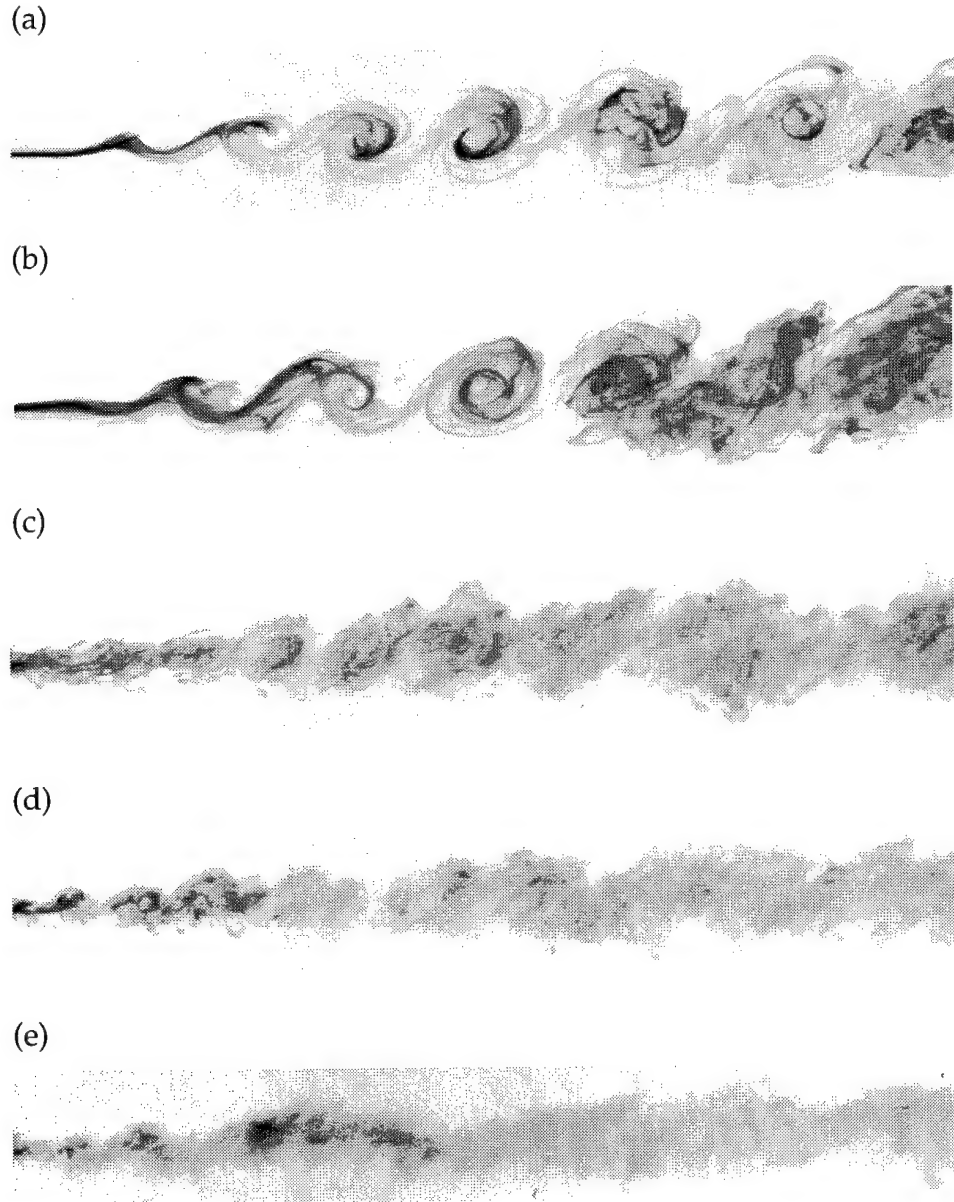
Smoke was used to visualize the flow, to help determine if the insert was effective. We created smoke by burning a smoke-generating, non-toxic incense material in a combustion chamber. We pressurized the chamber to 70 kPa and extended a hose from the top of the combustion chamber to a manifold via a heat exchanger. The manifold distributed the smoke to four smaller lines, which emptied into a plenum inside the wind tunnel insert. We formed the insert plenum from the gap left by the plexiglass sheet, as described in section 3.1.2. The 0.00318-m gap was approximately 0.4 m wide and 1.22 m deep, creating a plenum volume of 1.55 liters. About 0.4 m upstream of the trailing edge, cut into the high speed side of the insert, is a 0.00159-m-wide, 0.2-m-long slit, where the smoke seeps into the flow at about 0.1 m/s. A flash bulb, placed downstream but facing upstream, illuminated the smoke as it was convected downstream. Figure 4 shows a series of such captured images. In each case, the wind tunnel was running at different speeds, indicated by the blowers speed in revolutions per minute (rpm).

The images were captured on 200-ASA film, with the  $f$ -stop set to 2.5 and the shutter speed set to 30. This is a relatively slow shutter speed, but with the low ASA film, this was the fastest shutter speed it was possible to use without losing the image. As a result, the higher velocity flows (fig. 4d and e) are somewhat smeared. Despite these limitations, spanwise vortical concentrations are still visible at the wind tunnel's highest speed.

## 3.2 **Hot-Wire Measurements**

Hot-wire anemometry is still the method used most often to measure the fluctuating velocity components of fluids. The high spatial resolution, fast response time, and low fabrication cost make hot wire sensors ideal for this investigation (Blackwelder, 1981). A series of single hot-wire measurements were made to characterize the flow in the wind tunnel, and then compared to the velocity characteristics of the results of Rogers and Moser (1994). It was discovered that the contraction side of the splitter plate required a trip to produce a turbulent boundary layer. Once established, the resulting velocity measurements were very close to the numerical results, as well as the results of Bell and Mehta (1990).

Figure 4. Streaklines from smoke shown using flashbulb with 200-ASA film: (a) 200 rpm, (b) 270 rpm, (c) 400 rpm, (d) 500 rpm, and (e) 700 rpm.



### 3.2.1 Measurement Results

A single hot wire was used to obtain instantaneous velocity measurements for the condition of upstream velocity  $U_{\infty} = 2.46$  m/s. The measurements were made at 0.005-m increments along a transverse line ranging from 0.15 m below (slow side) to 0.15 m above (fast side) the trailing edge. A complete set of measurements was obtained from just at the downstream trailing edge of the splitter plate ( $x_1 \approx 0$  m) to 1.1 m downstream, at 0.1-m intervals. The hot wire was moved to each vertical location with a traverse mechanism, and held for 60 s while the acquisition system sampled at 1 kHz. The data were analyzed for mean velocity, variance, standard deviation, skewness, and kurtosis. Figures 5a through e are the resulting plots.

Figure 5. Contour results of single hot-wire measurements:  
(a) mean velocity,  
(b)  $\partial U_1 / \partial x_2$ ,  
(c) variance.

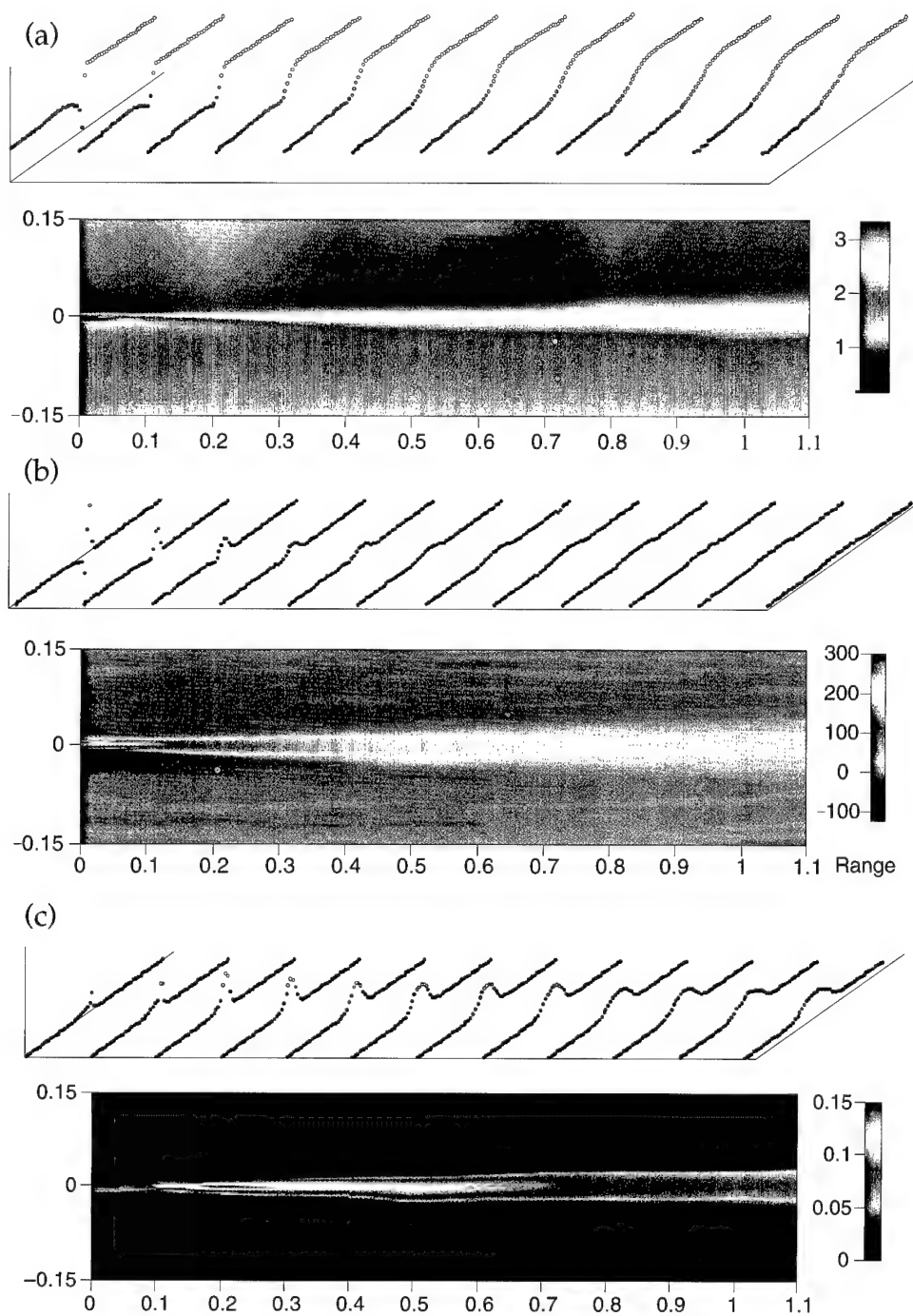
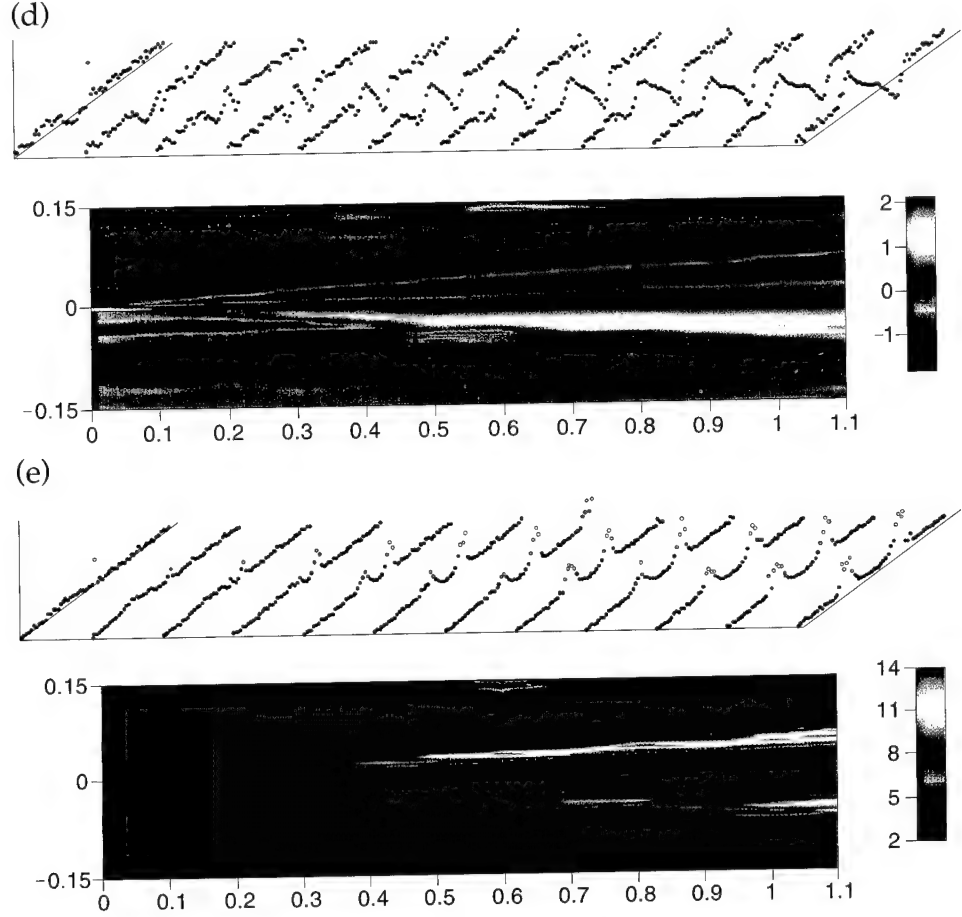


Figure 5. Contour results of single hot-wire measurements: (d) skewness, and (e) kurtosis.



These figures consist of a three-dimensional data point plot, followed by a colored contour plot. The data points are plotted in a perspective view with the measured quantity represented as vertical height. The color bar on the right of each contour plot shows the spatial variation of each flow component. They show that the mixing layer grows linearly from about 0.3 m downstream of the splitter plate. Table 1 lists some resulting parameters. These results are discussed later.

There are two convenient lengths for scaling that can be derived from the mean velocity distribution. The vorticity thickness  $\delta_\omega$  is defined as

$$\delta_\omega \equiv \frac{\Delta U}{\left. \frac{\partial \bar{U}_1}{\partial x_1} \right|_{\max}} . \quad (1)$$

It is an appropriate measure of the growth of the turbulent mixing layer. The momentum thickness  $\theta$  is defined in the usual way, as

$$\theta = \int_{-\infty}^{\infty} \left[ \frac{1}{4} - \left( \frac{\bar{U}_1 - U_c}{\Delta U} \right)^2 \right] dx_2 , \quad (2)$$

Table 1. Characterization results.

Description	Variable	Numerical value
Free-stream velocity, fast	$U_h$	3.19 m/s
Free-stream velocity, slow	$U_l$	1.69 m/s
Velocity ratio	$U_l/U_h$	0.53
Convection velocity	$U_c$	2.44 m/s
Momentum thickness (m)	$\theta$	$-0.000504 \text{ m} + 0.0165 \times 1$
Reynolds number (based on $\theta$ )	$Re_\theta$	$80.7 + 1655.1/\text{m} \times 1$
Vorticity thickness (m)	$\delta_\omega$	$0.005484 \text{ m} + 0.06545 \times 1$
Reynolds number (based on $\delta_\omega$ )	$Re_\omega$	$427.99 + 6523.5/\text{m} \times 1$
Nondimensional growth rate of $\delta_\omega$	$r_\omega$	0.0531
Strouhal number	$St$	0.12
Wavelength	$\lambda$	0.133 m
Maximum turbulence level	$\sqrt{u_1^2} _{\max}/\Delta U \times 100\%$	27.8 %

where  $U_c \approx 0.5(U_h + U_l)$ , and represents the flow of momentum through the mixing layer compared to that which would occur if no shear layer was present. Since the measurements were taken at 0.005-m intervals in the  $x_2$  direction, the momentum thickness was calculated discretely as

$$\theta = \sum_i \left[ \frac{1}{4} - \left( \frac{\bar{U}_{1,i} - U_c}{\Delta U} \right)^2 \right] 0.005 \text{ m} , \quad (3)$$

where  $i$  is the number of points and associated location along  $x_2$ . Each length scale can be used in a Reynolds number. Two such Reynolds numbers are defined: the Reynolds number based on vorticity thickness,

$$Re_{\delta_\omega} = \frac{\Delta U \delta_\omega}{\nu} , \quad (4)$$

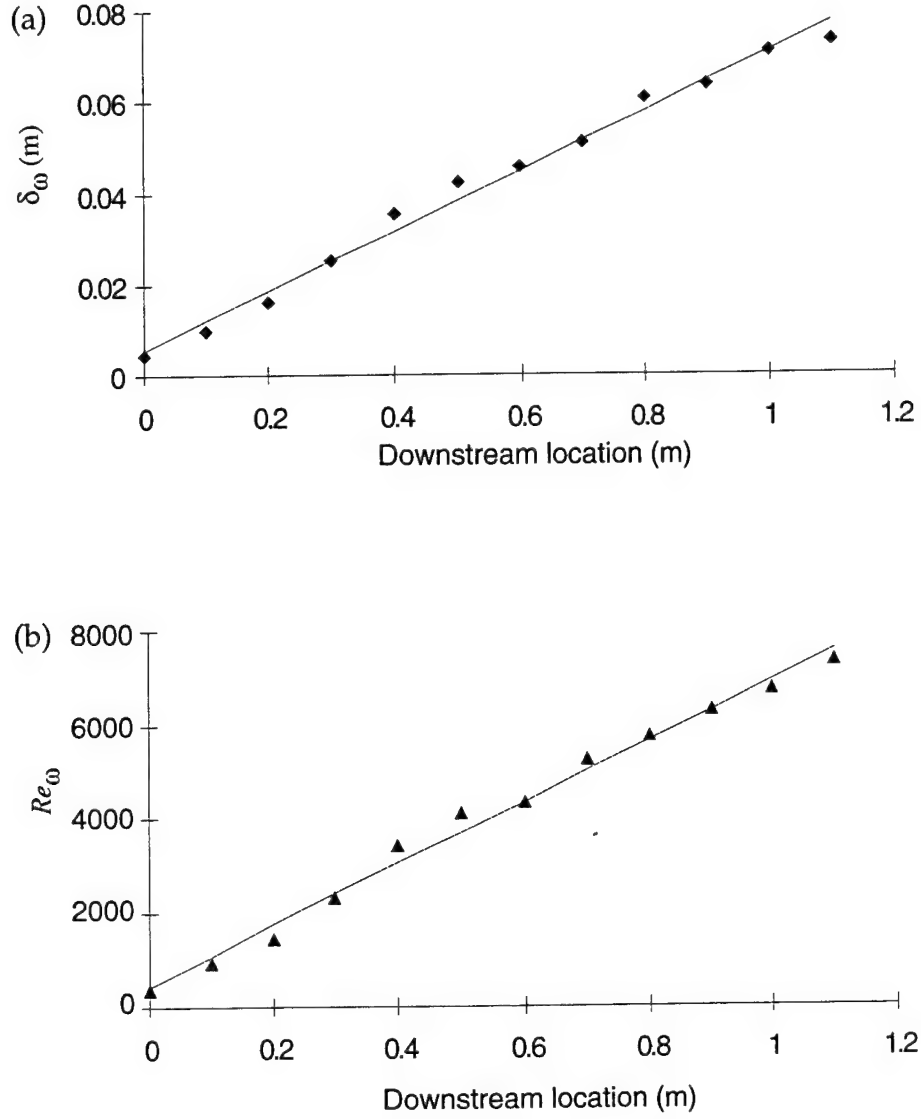
and the Reynolds number based on momentum thickness,

$$Re_\theta = \frac{\Delta U \theta}{\nu} . \quad (5)$$

The momentum thickness is often used for self-similar scaling rather than vorticity thickness because momentum thickness is less sensitive to statistical noise. Other investigators have used the vorticity thickness to nondimensionally scale the vertical distance across the shear layer. The rationale is that this scaling takes into account some of the deviation from linear growth of the shear layer near the trailing edge. Figure 6 shows growth of the vorticity thickness with distance downstream, and the corresponding growth of the Reynolds numbers based on  $\delta_\omega$ . Each plot also has a least-squares linear fit to the data.

The growth of the vorticity thickness and the related Reynolds number are linear. The least-squares linear fit of the data yields a growth rate,  $\partial \delta_\omega / \partial x_2$  (the slope), and the initial value (intercept). The least-squares linear fit to

Figure 6. Growth of  
(a) vorticity thickness  
with thickness  
downstream and  
(b) Reynolds number.

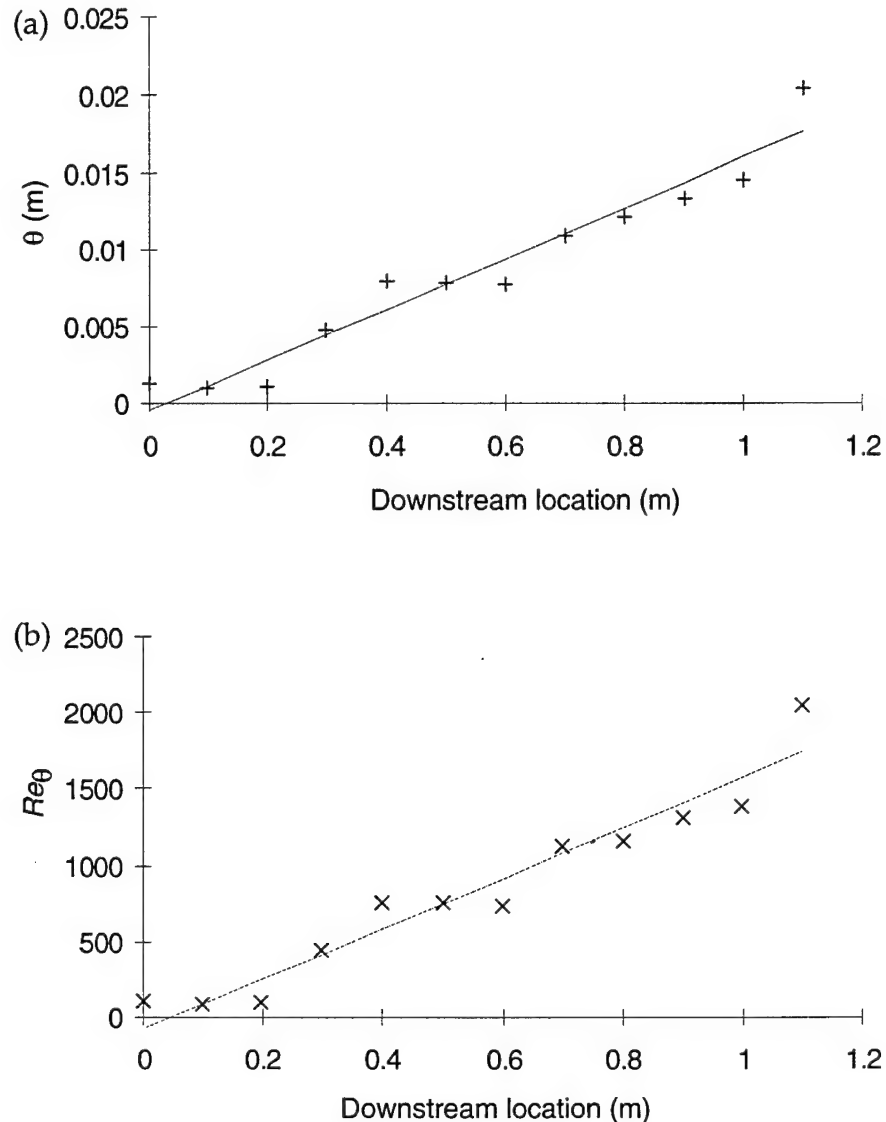


the data set appear in table 1. The nondimensional growth rate of the vorticity thickness ( $r_\omega$ ) is defined as

$$r_\omega = \frac{U_c}{\Delta U} \frac{\partial \delta_\omega}{\partial x_2} . \quad (6)$$

Using the least-squares fit for the slope (0.06545 m/m),  $r_\omega = 0.1065$ . This is a little higher than the value of 0.098 from Wygnanski and Fiedler (1970). Brown and Roshko (1974) attained a value of 0.0905. Their lower value may be due to the fact that Brown and Roshko's Reynolds number, based on vorticity thickness ( $\approx 342000 x_1$ ), was much higher due to their increased convective velocity (factor of 2) and density (factor of 7). The simulation by Rogers and Moser (1994) resulted in  $r_\omega = 0.0672$ . Similar plots were made for the momentum thickness,  $\theta$ , along with its related Reynolds number (see fig. 7).

Figure 7. Growth of  
(a) momentum  
thickness with  
thickness  
downstream and  
(b) associated  
Reynolds number.



From the trailing edge out to about 0.3 m, the wake defect caused by the screen on the expansion produces mean velocity profiles that are not similar to the profiles further downstream, as can be seen in figure 5a. In fact, the profiles behave more like the combination of two flat-plate boundary layers and the wake from a bluff body. The momentum thickness may be more appropriately calculated (and is here) out to 0.2 m downstream of the splitter plate. Self-similarity is attained by 0.3 m downstream, and the momentum thickness grows as expected. Kim (1989) shows a linearly growing momentum thickness starting at 0.3 m. Winant and Browand (1974) show the momentum thickness evolving from the trailing edge. This is easily attributed to the different method employed in creating the mixing layer from two separate flows, and exploiting the lower kinematic viscosity of water. Winant et al. explained that  $\theta$  initially grows as the square root of the downstream distance. Where the mixing layer transitions to turbulence,  $\theta$  grows linearly. The conditions of Rogers and Moser (1994) was an initial  $Re_\omega$  and  $Re_\theta$  of 1370 and 800, growing to 10,800 and 2,420, respectively.

An important test for performance of the facility to generate a mixing layer matching the numerical conditions of Rogers and Moser (1994) is whether the data collapses in a self-preserving manner. Rogers and Moser collapsed the mean velocity data by plotting the nondimensional mean streamwise velocity  $(\bar{U}_1 - U_c)/\Delta U$ , plotted against the nondimensional vertical distance,  $\xi = x_2/\theta$ , where  $\Delta U \equiv U_h - U_l$ . As shown in figure 8, the mean velocity from the preliminary study shows self-similarity from about 0.3 m downstream of the splitter plate. The collapse of the data is in reasonable agreement with the results of Rogers and Moser.

Rogers and Moser indicate that a more sensitive indicator of self-similarity is the collapse of the Reynolds stress profiles  $\overline{u'u'}$  with  $\xi$ . The appropriate scale used was  $\Delta U^2$ . Their data showed a well-collapsed distribution of the streamwise Reynolds normal stress at five different locations within their self-similar regime. Figure 9 shows the normalized data results from this preliminary study. Much like the results of Roger and Moser, the data at 0.9 through 1.1 m very nearly collapse, closely matching the results of Rogers and Moser's peak self-similar value of  $\overline{u'u'}/\Delta U^2$ , going to 0 at  $x \approx \pm 4$ .

Figure 8. Normalized mean velocity profiles.

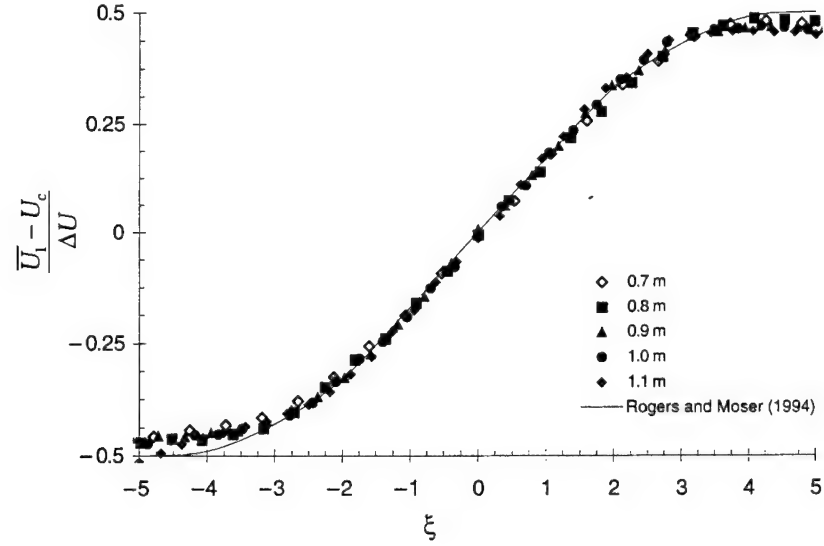
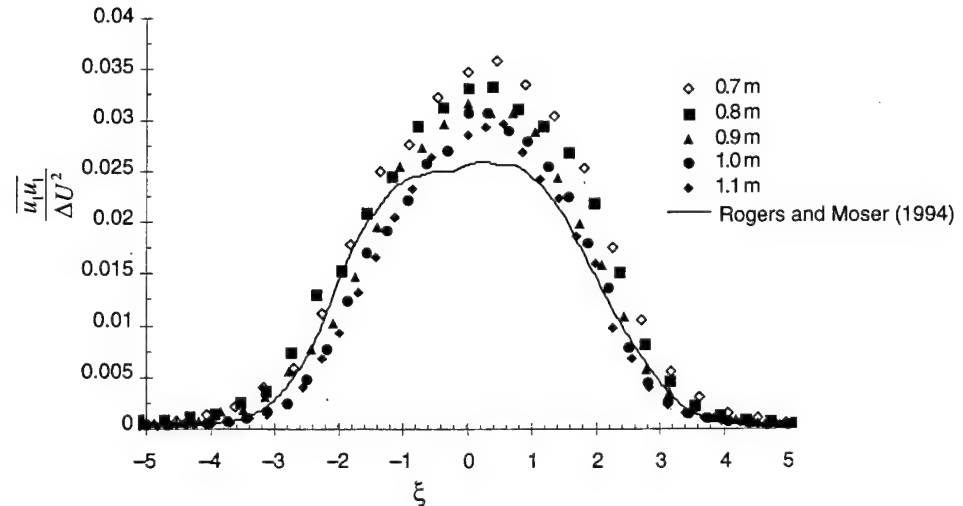


Figure 9. Normalized Reynolds normal stress in streamwise direction.



### 3.2.2 Initial Conditions

An initial profile of the mean streamwise flow 0.002 m downstream of the splitter plate is shown in figure 10. One can see that the mean flow exhibits a larger boundary layer profile on the expansion side, and the variance seems to grow with the velocity defect. It is theorized that there is some separation along the concave curvature of the splitter plate. On the contraction side, the boundary layer is initially laminar and small.

The streamwise mean velocity and variance data of the expansion side of the splitter plate were plotted to evaluate the similarity to the expected logarithmic form given by Clauser (1956) fit to a turbulent boundary layer on a smooth, solid surface. The results are shown in figure 11, where the velocity is normalized by the *friction velocity*  $u_\tau$ , defined as

$$u_t = \sqrt{\frac{\partial U_1}{\partial x_2} \frac{\nu}{\rho}} , \quad (7)$$

where the velocity and length are normalized as

$$u^+ = \frac{u_1}{u_\tau} , \quad (8)$$

$$y^+ = \frac{x_2 u_\tau}{\nu} .$$

Comparison of the resulting fit indicates the mean streamwise velocity and the variance with Balint, Wallace, and Vukoslavcevic (1991) are not behaving exactly as a turbulent boundary layer on a flat plate. There is obviously a contribution from the relaxing pressure gradient from the splitter plates curvature. It is expected that the velocities would not collapse as neatly as the flat plate family, because of an existing, relaxing pressure gradient.

Clauser (1956) named a similar class of turbulent boundary layer flows with pressure gradients as *equilibrium pressure gradient flows*. These were

Figure 10. Initial streamwise profiles.

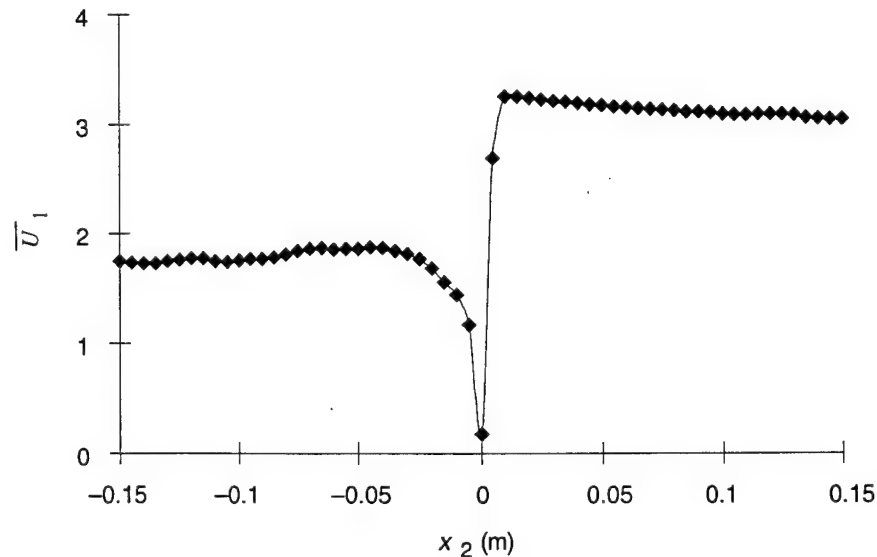
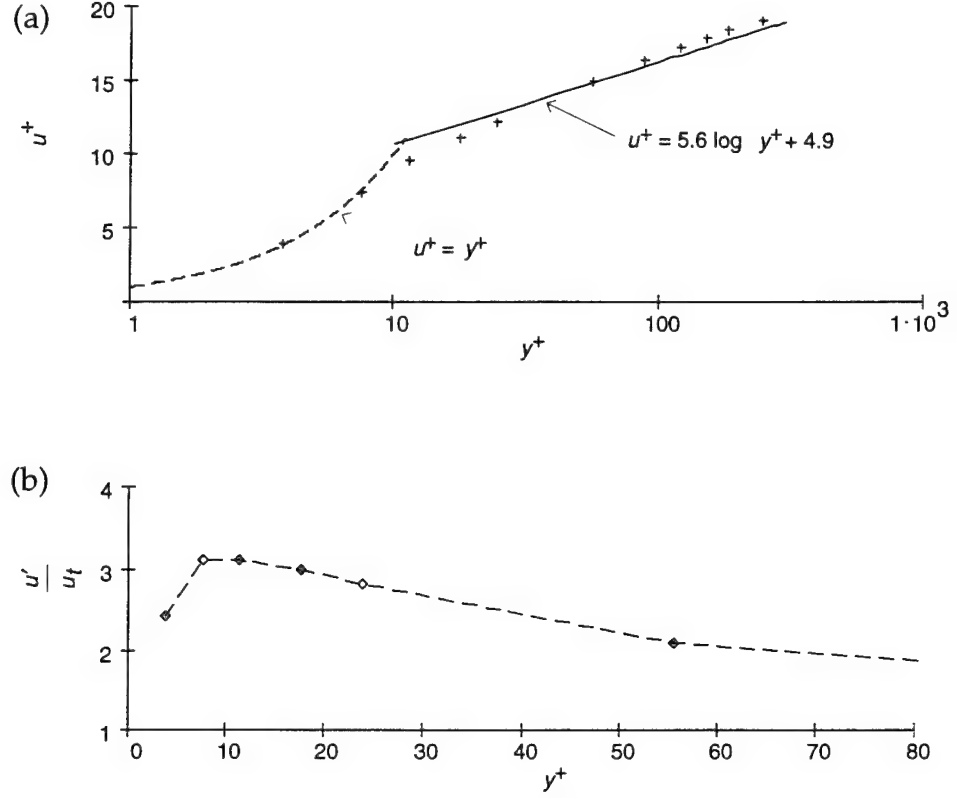


Figure 11. Boundary layer profile of expansion surface:  
(a) mean streamwise velocity and  
(b) variance profile.



used to generalize turbulent boundary layer flows around curved surfaces, much like the splitter plate. Coles (1956) extended the *law of the wake*,

$$u^+ = 5.6 \log y^+ + 4.9 + \frac{\Pi}{K} W\left(\frac{\delta}{x_2}\right), \quad (9)$$

to *equilibrium pressure gradient* by letting the wake parameter,  $P$ , be a function of the displacement thickness, wall shear, and the pressure gradient:

$$\Pi = f\left(\frac{\delta^*}{\tau_w} \frac{dP}{dx_2}\right). \quad (10)$$

Here,  $\delta$  is the boundary layer thickness;  $\delta^*$  is the *displacement thickness* and is defined as

$$\delta^* \equiv \int_0^d \left(1 - \frac{U_1}{U_{1\infty}}\right) dx_2, \quad (11a)$$

while the wall shear is defined as

$$\tau_w = \mu \frac{\partial U_1}{\partial x_2}. \quad (11b)$$

White (1974) proposed that

$$\Pi = 0.8 \left( \frac{\delta^*}{\tau_w} \frac{dP}{dx_2} + 0.5 \right)^{3/4}. \quad (12)$$

Letting  $\kappa = 0.41$  (Schetz, 1984), Cole (1956) proposed that

$$W\left(\frac{\delta}{x_2}\right) = 2 \sin^2\left(\frac{\pi}{2} \frac{x_2}{\delta}\right), \quad (13)$$

resulting in the *law of the wake* as

$$u^+ = 5.6 \log y^+ + 4.9 + 3.9024 \left( \frac{\delta^*}{\tau_w} \frac{dP}{dx_2} \right)^{3/4} \sin^2\left(\frac{\pi}{2} \frac{\delta}{x_2}\right). \quad (14)$$

This law states that a pressure gradient in the  $x_2$  direction greater in magnitude than that of a flat plate will result in larger values of  $u^+$ . The magnitude of the pressure gradient determines the degree of deviation from the smooth flat plate turbulent boundary layer profile. In this instance, on both sides of the splitter plate, the pressure gradient is relaxing with increasing  $x_1$ . As a result, the added value of the pressure gradient contributes to the small deviation from the Clauser fit (Clauser, 1956), as one can observe from figure 11b.

The variance of the untripped flow is already in excess of the expected values from Balint et al. (1991). Tripping the expansion side would create even greater variance and turbulent kinetic energy. A typical peak variance of a turbulent boundary layer is about  $u'/u_\tau = 3.12$  at  $y^+ \approx 11.4$ . In this case,  $u_\tau$  is estimated to be about 0.097 m/s.

This degree of turbulence originating from the expansion side of the splitter plate eliminated the possibility of performing the simulation with laminar initial conditions. The contraction side was tripped by placing a 0.01-m-diameter rod on the contraction surface about 0.1 m downstream of the splitter plate leading edge. The single sensor was used to measure the streamwise velocity on the contraction side about 0.005 m upstream of the trailing edge. Figure 12 shows the measurements obtained.

The boundary layer profile of the contraction side compares much more favorably with the results of Balint et al. (1991). This is because the relaxation of the pressure gradient is not as pronounced. On this side, a typical peak variance of a turbulent boundary layer is about  $u'/u_\tau = 2.37$  at  $y^+ \approx 12.4$ , and  $u_\tau$  is estimated to be about 0.19 m/s. Table 2 lists the boundary layer properties for each side. Each property is defined as

$$\begin{aligned} \frac{\partial U_1}{\partial x_2} \Big|_{x_2=0} &= \frac{u_\tau^2}{\nu}, \\ C_f &= 2 \frac{u_\tau^2}{U_{1,\infty}^2}, \end{aligned} \quad (15)$$

where  $C_f$  is the coefficient of drag.

Figure 12. Boundary layer profile of tripped contraction: (a) mean streamwise velocity and (b) variance profile.

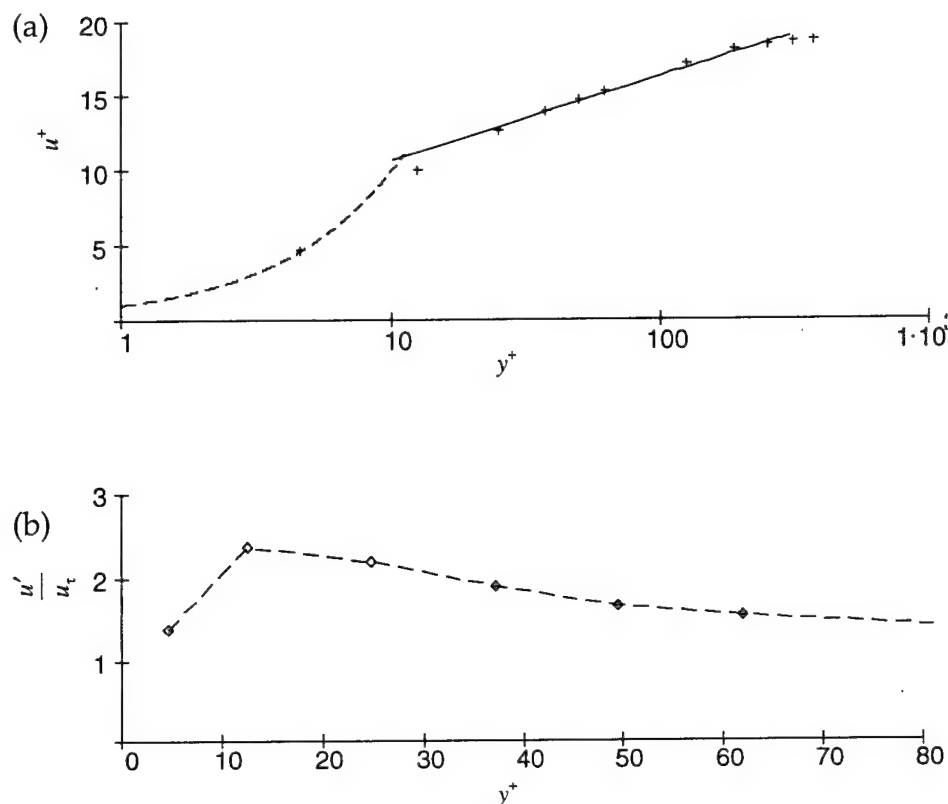


Table 2. Turbulent boundary layer.

Flow side	$u_\tau$ (m/s)	$\frac{\partial U_1}{\partial x_2} \Big _{x_2=0}$	$C_F$	$\frac{u'_1}{u_\tau} \Big _{\max}$	$\frac{u_\tau}{U_{1,\infty}}$
Expansion	0.097	$611.37 \text{ s}^{-1}$	0.005958	3.12	0.0546
Contraction	0.19	$2344.7 \text{ s}^{-1}$	0.005706	2.37	0.0534

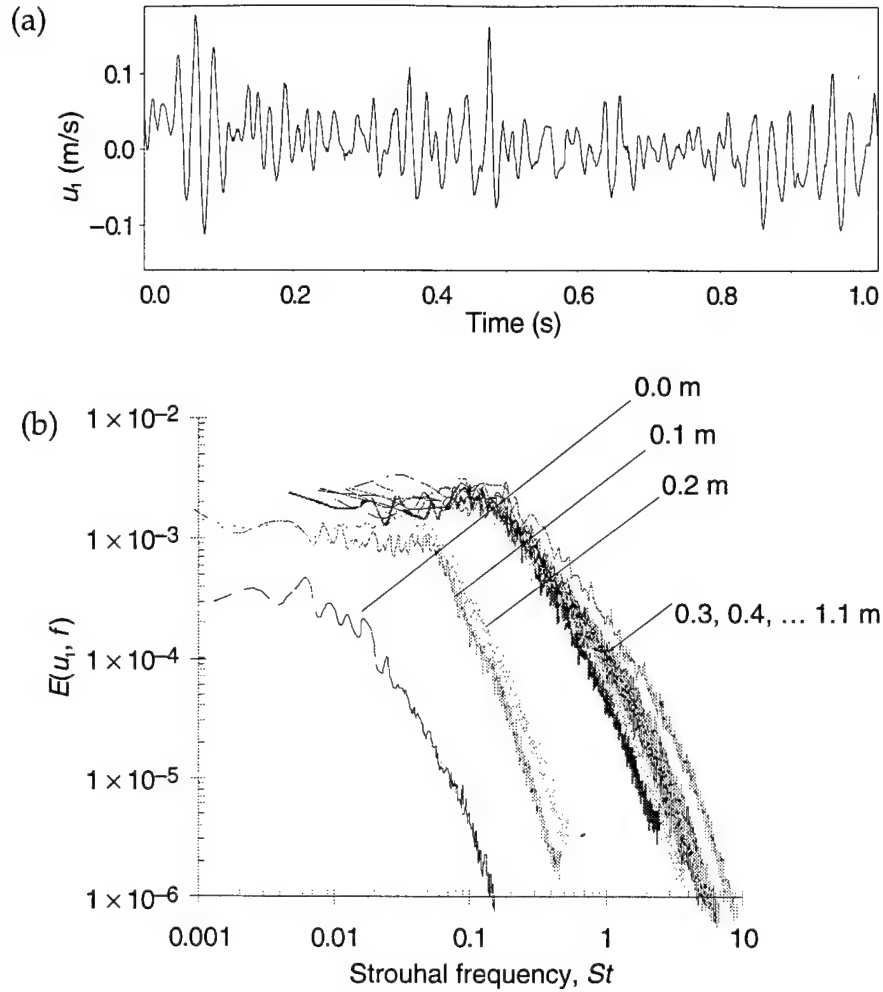
The effect of the pressure gradient is small. As a result, I decided to perform simulations with the contraction side tripped and the expansion side untripped. This allowed me to use our existing facilities to closely emulate the initial condition of a turbulent boundary layer matching the simulation of Rogers and Moser (1994).

### 3.3 Roller Passage

Most of the references discuss the frequency of the passage of the rollers. Kim (1989) showed the spectral content of the streamwise and transverse velocity components. His plots exhibited a smooth cresting between 30 and 40 Hz for the streamwise velocity spectrum, while there was a definitive peak at about 40 Hz for the transverse velocity component.

As seen in figure 4, there is strong visual evidence that rollers are produced in this facility. Figure 13a shows a sample of the fluctuating data, taken at the edge of the faster part of the shear layer, at  $x_1 = 0.2 \text{ m}$ .

Figure 13. Sample data and normalized spectrum: (a) sample of fluctuating velocity data from single hot-wire anemometer and (b) normalized power spectrum of velocity data.



There is a dominant frequency from the coherent spanwise vorticity continued in the rollers. If the frequency of passage of the rollers is directly related to the downstream distance, one could collapse the spectral plots by use of the mixing layer scale,  $\theta$  or  $\delta_w$ . Figure 13b shows the spectral energy content of this data. Note the apparent collapse of the spectral profiles taken from  $x_1$  from 0.3 to 1.1 m. This is similar to the result of Hussain and Zaman (1985). Typically, the dominant periodicity of the passage of the rollers,  $f_0$ , is expressed nondimensionally as the Strouhal number

$$St = \frac{\theta f_0}{U_c} . \quad (15)$$

The resulting Strouhal number, using  $\theta$  as the length scale, is  $St = 0.12$  at 0.3 to 1.1 m downstream of the trailing edge. Since the rollers convect downstream at an approximately constant velocity,  $St$  will remain constant. The  $St$  does vary from  $x_1 = 0.3$  m to 1.1 m, suggesting evidence of pairing; the rollers grow linearly, yet convect downstream at a constant velocity, eventually crowding, and then pairing occurs. This mechanism is what allows  $\lambda$  to remain constant in the self-similar region of the flow. As pointed out in section 1, the mixing layer exhibits properties that are independent of downstream location when scaled with the appropriate local length scale.

## 4. Conclusions and Recommendations

A thorough measurement of the structure and dynamics of the streamwise velocity in a turbulent plane mixing layer was taken, using a single-sensor hot-wire probe. The results of the measurements were compared against a theoretical computation of a similar flow by Rogers and Moser (1994). This investigation demonstrated that the wind tunnel facility, with the splitter plate insert and screen, can create the turbulent plane mixing layer environment with standard velocity statistical properties similar to that in the numerical experiment by Rogers and Moser (1994). I anticipate that stations further downstream of the last measurement station will be well into the self-similar region described by Rogers and Moser.

These results dictate that the use of multisensor probes with 4, 9, or 12 sensor arrays to measure the velocity vector components, the velocity gradients, and the vorticity would be of high quality and value. These probes are capable of measuring minute volumes, such that the probe dimensions are approximately of the same order as the anticipated Kolmogoroff length scale (using the isotropic turbulence assumption for calculation of the dissipation rate). Thus, high-quality measurements could be made of the turbulence properties and associated statistics. Conditional averaging could additionally be used to evaluate the distributions of turbulent kinetic energy, enstrophy, dissipation rate, amongst other properties. Such measurements could be compared against the results of prior literature, and could then be extended. Such extensions would enhance the present understanding of turbulence in coherent structures, increasing the capability of improving turbulence models for computational fluid dynamics, and would contribute to the body of knowledge in turbulent fluid dynamics.

## 5. References

- ALGOR, Inc., February 1992, *Fluid Flow Release Notes: Introduction to Incompressible Fluid Dynamics*, Pittsburgh PA.
- Ashurst, W. T., and E. Meiburg, 1988, "Three-Dimensional Shear Layers via Vortex Dynamics," *Journal of Fluid Mechanics* **189**, pp 87-116.
- Balint, J.-L., J. M. Wallace, and P. Vukoslavcevic, 1991, "The Velocity and Vorticity Vector Fields of a Turbulent Boundary Layer: Part 2. Statistical properties," *Journal of Fluid Mechanics* **228**, p 53.
- Batt, R. G., 1977, "Turbulent Mixing of Passive and Chemically Reacting Species in a Low-Speed Shear Layer," *Journal of Fluid Mechanics* **82**, p 53.
- Bell, J. H., and R. D. Mehta, 1990, "Development of a Two-Stream Mixing Layer from Tripped and Untripped Boundary Layers," *AIAA Journal* **28**, p 2034.
- Bell, J. H., M. W. Plesniak, and R. D. Mehta, 1992, "Spanwise Averaging of Plane Mixing Layer Properties," *AIAA Journal* **30**, p 835.

- Bernal, L. P. and A. Roshko, 1986, "Streamwise Vortex Structure on Plane Mixing Layers," *Journal of Fluid Mechanics* **170**, pp 499–525,
- Blackwelder, R. F., 1981, "An Introduction to Hot-Wire and Hot-Film Anemometry," *Methods of Experimental Physics: Fluid Dynamics, Part A*, edited by R. Emrich, Academic Press, New York, pp 259–314.
- Bradshaw, P., 1966, "The Effect of Initial Conditions on the Development of a Free Shear Layer," *Journal of Fluid Mechanics* **26**, pp 225–236.
- Browand, F. K., and T. R. Troutt, 1980, "A Note on Spanwise Structure in the Two-Dimensional Mixing Layer," *Journal of Fluid Mechanics* **97**, pp 771–781.
- Brown, L. B. and A. Roshko, 1974, "On Density Effects and Large Structure in the Turbulent Mixing Layers," *Journal of Fluid Mechanics* **64**, pp 775–816.
- Chandrsuda, A., R. D. Mehta, A. D. Weir, and P. Bradshaw, 1978, "Effect of Free-Stream Turbulence on Large Structure in Turbulent Mixing Layers," *Journal of Fluid Mechanics* **85**, pp 693–704.
- Clauser, F. H., 1956, "The Turbulent Boundary Layer," *Advances in Applied Mechanics* **4**, Academic Press, New York.
- Coles, D., 1956, "The Law of the Wake in the Turbulent Boundary Layer," *Journal of Fluid Mechanics* **1**, pp 191–226.
- Corcos, G. M., and S. J. Lin, 1984, "The Mixing Layer: Deterministic Models of a Turbulent Flow: Part 2. The Origin of the Three-Dimensional Motion," *Journal of Fluid Mechanics* **139**, pp 67–95.
- Corcos, G. M., and F. S. Sherman, 1984, "The Mixing Layer: Deterministic Models of a Turbulent Flow: Part 1. Introduction and the Two-Dimensional Flow," *Journal of Fluid Mechanics* **139**, pp 29–65.
- Dimotakis, P. E., and G. L. Brown, 1976, "The Mixing Layer at High Reynolds Number: Large-Structure Dynamics and Entrainment," *Journal of Fluid Mechanics* **78**, pp 535–560.
- Ghoniem, A. F., and G. Heidarinejad, 1991, "Effect of Damkohler Number on the Reactive Zone Structure in a Shear Layer," *Combustion and Flame* **83**, pp 1–16.
- Hernan, M. A., and J. Jiminez, 1982, "Computer Analysis of a High-Speed Film of the Plane Mixing Layer," *Journal of Fluid Mechanics* **119**, pp 323–345.
- Ho, C.-M., and L.-S. Huang, 1982, "Subharmonic and Vortex Merging in Mixing Layers," *Journal of Fluid Mechanics* **119**, pp 443–473.
- Huang, L.-S., and C.-M. Ho, 1990, "Small-scale Transition in a Plane Mixing Layer," *Journal of Fluid Mechanics* **210**, pp 475–500.
- Hussain, A.K.F.M., and K.B.M.Q. Zaman, 1985, "An Experimental Study of Organized Motion in the Turbulent Plane Mixing Layer," *Journal of Fluid Mechanics* **159**, pp 85–104.

Jacobs, P. A., and D. I. Pullin, 1989, "Multiple-Contour-Dynamic Simulation of Eddy Scales in the Plane Shear Layer," *Journal of Fluid Mechanics* **199**, pp 89–124.

Jimenez, J., 1983, "A Spanwise Structure in the Plane Shear Layer," *Journal of Fluid Mechanics* **132**, pp 319–336.

Kelly, R. E., 1967, "On the Stability of an Inviscid Shear Layer Which is Periodic in Space and Time," *Journal of Fluid Mechanics* **27**, pp 657–689.

Kim, J.-H., 1989, "Wirbelstärkemessungen in einer turbulenten Scherschicht," Ph.D. dissertation, Physikalische Ingenieurwissenschaften der Technischen Universität Berlin.

Lang, D. B., 1985, "Laser Doppler Velocity and Vorticity Measurements in Turbulent Shear Layers," Ph.D. dissertation, California Institute of Technology.

Lasheras, J. C., J. S. Cho, and T. Maxworthy, 1986, "On the Origin and Evolution of Streamwise Vortical Structures in a Plane, Free Shear Layer," *Journal of Fluid Mechanics* **172**, pp 231–258.

Lasheras, J. C., and H. Choi, 1988, "Three-Dimensional Instability of a plane Free Shear Layer: An Experimental Study of the Formation and Evolution of Streamwise Vortices," *Journal of Fluid Mechanics* **189**, pp 53–86.

Metcalf, R. W., A.K.M.F. Hussain, S. Menon, and M. Hayakawa, 1987, "Coherent Structures in a Turbulent Mixing Layer: A Comparison Between Direct Numerical Simulation and Experiments," *Turbulent Shear Flows 5*, eds F. Durst, B. E. Launder, J. L. Lumley, F. W. Schmidt, and J. H. Whitelaw, Berlin, pp 110–123.

Metcalf, R. W., S. A. Orszag, M. E. Brachet, S. Menon, and J. J. Riley, 1987, "Secondary Instability of a Temporally Growing Mixing Layer," *Journal of Fluid Mechanics* **184**, pp 207–243.

Miksad, R. W., 1972, "Experiment on the Nonlinear Stages of Free-Shear Layer Transition," *Journal of Fluid Mechanics* **56**, pp 695–719.

Moser, R. D., and M. M. Rogers, May 1991, "Mixing Transition and the Cascade to Small Scales in a Plane Mixing Layer," *Physics of Fluids and Fluid Dynamics* **3**, pp 1128–1134.

Moser, R. D., and M. M. Rogers, October 1992, "Coherent Structures in a Simulated Turbulent Mixing Layer," *International Union of Theoretical and Applied Mechanics Symposium on Eddy Structure Identification*, Elsevier Science Publishers, North Holland.

Moser, R. D., and M. M. Rogers, 1993, "The Three-Dimensional Evolution of a Plane Mixing Layer: Pairing and Transition to Turbulence," *Journal of Fluid Mechanics* **247**, pp 275–320.

- Patnaik, R. T., F. S. Sherman, and G. M. Corcos, 1976, "A Numerical Simulation of Kelvin-Helmholtz Waves of Finite Amplitude," *Journal of Fluid Mechanics* **73**, pp 215-240.
- Pierrehumbert, R. T. and S. E. Widnall, 1982, "The Two- and Three-Dimensional Instabilities of a Spatially Periodic Shear Layer," *Journal of Fluid Mechanics* **114**, pp 59-82.
- Riley, J. J., and R. W. Metcalf, 1980, "Direct Numerical Simulation of a Perturbed Turbulent Mixing Layer," AIAA Paper 80-0274.
- Rogers, M. M., and R. D. Moser, 1992, "The Three-Dimensional Evolution of a Plane Mixing Layer: the Kelvin-Helmholtz Rollup," *Journal of Fluid Mechanics* **243**, pp 183-226.
- Rogers, M. M., and R. D. Moser, February 1994, "Direct Simulation of a Self-Similar Turbulent Mixing Layer," *Physics of Fluids and Fluid Dynamics* **6**, pp 903-923.
- Schetz, J. A., 1984, *Foundations of Boundary Layer Theory for Momentum, Heat, and Mass Transfer*, Prentice Hall, Inc., New Jersey.
- Spalart, P. R., 1988, "Direct Simulation of a Turbulent Boundary Layer up to  $R_\theta = 1410$ ," *Journal of Fluid Mechanics* **187**, pp 61-98.
- Vukoslavcevic, P., J. M. Wallace, and J.-L. Balint, 1991, "The Velocity and Vorticity Fields of a Turbulent Boundary Layer: Part 1. Simultaneous Measurement by Hot-Wire Anemometry," *Journal of Fluid Mechanics* **228**, pp 25-51.
- Winant, C. D., and F. K. Browand, 1974, "Vortex Pairing: the Mechanism of Turbulent Mixing-Layer Growth at Moderate Reynolds Number," *Journal of Fluid Mechanics* **63**, pp 237-255.
- Wynanski, I., and H. E. Fiedler, 1970, "The Two-Dimensional Mixing Region," *Journal of Fluid Mechanics* **41**, pp 327.

## Distribution

Admnstr  
Defns Techl Info Ctr  
Attn DTIC-OCP  
8725 John J Kingman Rd Ste 0944  
FT Belvoir VA 22060-6218

Central Intllgnc Agency Dir DB Standard  
Attn GE 47 QB  
Washington DC 20505

Chairman Joint Chiefs of Staff  
Attn J5 R&D Div  
Washington DC 20301

Defns Intllgnc Acgy  
Attn DT 2 Wpns & Sys Div  
Washington DC 20301

Defns Special Weapons Agcy  
Attn D Myers  
Attn Dr McFarland  
Attn LCOL A Kuehn  
Attn LCOL J Hodge  
Attn Techl Lib  
Attn WEL Collateral Effects  
6801 Telegraph Rd  
Alexandria VA 22310-3398

Dir of Defns Rsrch & Engrg  
Attn DD TWP  
Attn Engrg  
Washington DC 20301

Ofc of the Dir Rsrch and Engrg  
Attn R Menz  
Pentagon Rm 3E1089  
Washington DC 20301-3080

Ofc of the Secy of Defns  
Attn ODDRE (R&AT) G Singley  
Attn ODDRE (R&AT) S Gontarek  
The Pentagon  
Washington DC 20301-3080

OIR CSB CRB  
Attn A M Jones  
RB 1413 OHM  
Washington DC 20505

OSD  
Attn OUSD(A&T)/ODDDR&E(R) J Lupo  
The Pentagon  
Washington DC 20301-7100

Commanding Officer  
Attn NMCB23  
6205 Stuart Rd Ste 101  
FT Belvoir VA 22060-5275

Army Rsrch Ofc  
Attn AMXRO-GS Bach  
Attn Techl Lib  
PO Box 12211  
Research Triangle Park NC 27709

CECOM  
Attn PM GPS COL S Young  
FT Monmouth NJ 07703

CECOM RDEC Elect System Div Dir  
Attn J Niemela  
FT Monmouth NJ 07703

CECOM  
Sp & Terrestrial Commctn Div  
Attn AMSEL-RD-ST-MC-M H Soicher  
FT Monmouth NJ 07703-5203

Dir of Chem & Nuc Ops DA DCSOPS  
Attn Techl Lib  
Washington DC 20310

Dpty Assist Secy for Rsrch & Techl  
Attn SARD-TR R Chait Rm 3E476  
Attn SARD-TT D Chait  
Attn SARD-TT F Milton Rm 3E479  
Attn SARD-TT K Kominos  
Attn SARD-TT R Reisman  
Attn SARD-TT T Killion  
Attn SARD-TT C Nash Rm 3E479  
The Pentagon  
Washington DC 20301-0103

Hdqtrs Dept of the Army  
Attn DAMO-FDT D Schmidt  
400 Army Pentagon Rm 3C514  
Washington DC 20301-0460

## Distribution

US Army Engrg Div  
Attn HNDED FD  
PO Box 1500  
Huntsville AL 35807

US Army Matl Cmnd  
Dpty CG for RDE Hdqtrs  
Attn AMCRD BG Beauchamp  
5001 Eisenhower Ave  
Alexandria VA 22333-0001

US Army Matl Cmnd  
Prin Dpty for Acquisition Hdqtrs  
Attn AMCDCG-A D Adams  
5001 Eisenhower Ave  
Alexandria VA 22333-0001

US Army Matl Cmnd  
Prin Dpty for Techlgy Hdqtrs  
Attn AMCDCG-T M Fisette  
5001 Eisenhower Ave  
Alexandria VA 22333-0001

US Army Mis & Spc Intllgnc Ctr  
Attn AIAMS YDL  
Redstone Arsenal AL 35898-5500

US Army NGIC  
Attn Rsrch & Data Branch  
220 7th Stret NE  
Charlottesville VA 22901-5396

US Army Nuc & Cheml Agency  
7150 Heller Loop Ste 101  
Springfield VA 22150-3198

US Army Rsrch Ofc  
Attn AMXRO-ICA B Mann  
PO Box 12211  
Research Triangle Park NC 27709-2211

US Army Strtgc Defns Cmnd  
Attn CSSD H MPL Techl Lib  
Attn CSSD H XM Dr Davies  
PO Box 1500  
Huntsville AL 35807

US Military Academy  
Dept of Mathematical Sci  
Attn MAJ D Engen  
West Point NY 10996

USAASA  
Attn MOAS-AI W Parron  
9325 Gunston Rd Ste N319  
FT Belvoir VA 22060-5582

Chief of Nav OPS Dept of the Navy  
Attn OP 03EG  
Washington DC 20350

Nav Civil Engrg Lab  
Attn Code L51 J Tancreto  
Port Hueneme CA 93043-5003

Officer in Charge  
Nav Construction Battalion Ctr Civil Engrg Lab  
Attn Code L31 Techl Lib  
Port Hueneme CA 93041

Nav Rsrch Lab  
Attn Code 2027 Techl Lib  
Washington DC 20375

Nav Surface Warfare Ctr  
Attn Code B07 J Pennella  
17320 Dahlgren Rd Bldg 1470 Rm 1101  
Dahlgren VA 22448-5100

Ofc of Nav Rsrch  
Attn Code 23 A Faulstick  
800 N Quincy Stret  
Arlington VA 22217

US Nav Academy  
Attn LT D Fuller  
Attn P McCoy  
Attn Techl Lib  
572 Holloway Rd  
Annapolis MD 21402-5002

US Nav Academy  
Attn R Smith  
Attn T Butler  
363 Rickover Hall 590 Holloway Rd  
Annapolis MD 21402-5002

GPS Joint Prog Ofc Dir  
Attn COL J Clay  
2435 Vela Way Ste 1613  
Los Angeles AFB CA 90245-5500

## Distribution

Special Assist to the Wing Cmndr  
Attn 50SW/CCX Capt P H Bernstein  
300 O'Malley Ave Ste 20  
Falcon AFB CO 80912-3020

DARPA  
Attn B Kaspar  
Attn L Stotts  
Attn Techl Lib  
3701 N Fairfax Dr  
Arlington VA 22203-1714

US Dept of Energy  
Attn KK 22 K Sisson  
Attn Techl Lib  
Washington DC 20585

ARL Electromag Group  
Attn Campus Mail Code F0250 A Tucker  
University of Texas  
Austin TX 78712

George Mason University  
Insti for Computational Sci and Info  
Attn M Black  
Attn S Hanna  
Attn Techl Lib  
Fairfax VA 22030-444

MIT  
Attn Techl Lib  
Cambridge MA 02139

The Johns Hopkins Univ Applied Physic Lab  
Attn Techl Lib  
Johns Hopkins Rd  
Laurel MD 20707

Univ of Maryland  
Attn E Magrab  
Attn Engrg & Techl Lib  
Attn J Duncan  
Attn J Wallace  
Attn K Keiger  
Attn L Ong  
Attn P Bernard  
Attn R Calabrese  
Rm 2168 Engrg Classroom Bldg  
College Park MD 20742-5121

Forensics Technology International Corp  
Attn B Davis  
Attn D Malone  
Attn D Randall  
Attn J McDonough  
Attn J Reynolds  
2021 Research Dr  
Annapolis MD 21401

Olin Ordnance Product Material Control  
Attn J Kibiger  
Attn Techl Lib  
10101 9th Stret N  
ST Petersburg FL 33716

US Army Rsrch Lab  
Attn AMSRL-IS-CS A Mark  
Attn AMSRL-WT-TB P Muller  
Attn AMSRL-HR-SD L Ferguson  
Attn AMSRL-WM-TA A Milhalcin  
Attn AMSRL-WM-TB T Cline  
Attn AMSRL-WM-WB B Davis  
Attn AMSRL-WM-WB J Condon  
Attn AMSRL-WM-WB T Brown  
Attn AMSRL-WT-TB J Sullivan  
Attn AMSRL-WT-TB R Lottero  
Attn AMSRL-WT-TC De Rosset  
Aberdeen Proving Ground MD 21005-5055

US Army Rsrch Lab  
Attn AMSRL-CI-LL Techl Lib (3 copies)  
Attn AMSRL-CS-AL-TA Mail & Records  
Mgmt  
Attn AMSRL-CS-AL-TP Techl Pub (3 copies)  
Attn AMSRL-IS P Emmerman  
Attn AMSRL-IS-BP B Fornoff  
Attn AMSRL-IS-EE A Wetmore  
Attn AMSRL-IS-EE D Garvey  
Attn AMSRL-IS-EE J Martin  
Attn AMSRL-IS-EE K Deacon  
Attn AMSRL-IS-EE R Cianco  
Attn AMSRL-IS-EE R Loucks (4 copies)  
Attn AMSRL-IS-EE R Meyers  
Attn AMSRL-IS-EE R Pinnick  
Attn AMSRL-IS-EE S Niles

## Distribution

US Army Rsrch Lab (cont'd)  
Attn AMSRL-IS-ES P Gillespie  
Attn AMSRL-SE-SA J Gerber  
Attn AMSRL-SE-SA J Price  
Attn AMSRL-SE-SA K Tran

US Army Rsrch Lab (cont'd)  
Attn AMSRL-SE-SA M Fong  
Attn AMSRL-SE-SA T Pham  
Adelphi MD 20783-1197

<b>REPORT DOCUMENTATION PAGE</b>			Form Approved OMB No. 0704-0188	
Public reporting burden for this collection of information is estimated to average 1 hour per response, including the time for reviewing instructions, searching existing data sources, gathering and maintaining the data needed, and completing and reviewing the collection of information. Send comments regarding this burden estimate or any other aspect of this collection of information, including suggestions for reducing this burden, to Washington Headquarters Services, Directorate for Information Operations and Reports, 1215 Jefferson Davis Highway, Suite 1204, Arlington, VA 22202-4302, and to the Office of Management and Budget, Paperwork Reduction Project (0704-0188), Washington, DC 20503.				
1. AGENCY USE ONLY (Leave blank)		2. REPORT DATE September 1997		3. REPORT TYPE AND DATES COVERED Final, 10 October 1995 to 15 March 1996
4. TITLE AND SUBTITLE An Experimental Examination of the Streamwise Velocity in a Plane Mixing Layer using a Single Hot-Wire Sensor			5. FUNDING NUMBERS PE: 61102A	
6. AUTHOR(S) Richard B. Loucks				
7. PERFORMING ORGANIZATION NAME(S) AND ADDRESS(ES) U.S. Army Research Laboratory Attn: AMSRL-IS-EE 2800 Powder Mill Road Adelphi, MD 20783-1197			8. PERFORMING ORGANIZATION REPORT NUMBER ARL-TR-1391	
9. SPONSORING/MONITORING AGENCY NAME(S) AND ADDRESS(ES) U.S. Army Research Laboratory 2800 Powder Mill Road Adelphi, MD 20783-1197			10. SPONSORING/MONITORING AGENCY REPORT NUMBER	
11. SUPPLEMENTARY NOTES AMS code: 61110253A0011 ARL PR: 7FEJ60				
12a. DISTRIBUTION/AVAILABILITY STATEMENT Approved for public release; distribution unlimited.			12b. DISTRIBUTION CODE	
13. ABSTRACT (Maximum 200 words)  A single-sensor hot-wire probe was used to make streamwise measurements in a turbulent plane mixing layer. The mixing layer, with a velocity ratio of approximately 2:1, was created in an open return wind tunnel by the insertion of a curved splitter plate. Conditions were studied with the splitter plate boundary layers tripped. The single-sensor results demonstrate that this mixing layer has standard velocity field statistical properties. The data were taken at several Reynolds numbers in the fully turbulent flow downstream of the mixing point. The results from the tripped initial boundary layers/ fully turbulent conditions were compared with the temporally developing mixing layer direct numerical simulation results of Rogers and Moser (1994).  Rogers, M. M., and R. D. Moser, February 1994, "Direct Simulation of a Self-Similar Turbulent Mixing Layer," <i>Physics of Fluids and Fluid Dynamics</i> 6, pp 903-923.				
14. SUBJECT TERMS Fluid dynamics, turbulence, measurement, anemometer, mixing layer			15. NUMBER OF PAGES 35	
			16. PRICE CODE	
17. SECURITY CLASSIFICATION OF REPORT Unclassified	18. SECURITY CLASSIFICATION OF THIS PAGE Unclassified	19. SECURITY CLASSIFICATION OF ABSTRACT Unclassified	20. LIMITATION OF ABSTRACT UL	